Eur. Phys. J. Special Topics **223**, 373–387 (2014)

DOI: 10.1140/epjst/e2014-02097-x

THE EUROPEAN PHYSICAL JOURNAL SPECIAL TOPICS

Review

Density functional theory of heterogeneous crystallization

T. Neuhaus[1], A. Härtel[2], M. Marechal[3], M. Schmiedeberg[1,a], and H. Löwen[1,b]

[1] Institut für Theoretische Physik II: Weiche Materie, Heinrich-Heine-Universität Düsseldorf, Universitätsstraße 1, 40225 Düsseldorf, Germany
[2] Institute for Theoretical Physics, Universiteit Utrecht, Leuvenlaan 4, 3584 CE Utrecht, The Netherlands
[3] Institut für Theoretische Physik, Universität Erlangen-Nürnberg, Staudtstraße 7, 91058 Erlangen, Germany

Received 13 December 2013 / Received in final form 10 January 2014
Published online 28 February 2014

Abstract. This mini-review summarizes recent progress in describing heterogeneous crystallization processes and microstructure formation within microscopic classical density functional theory (DFT). After outlining the basic features of DFT, we discuss several applications ranging from the structure and thermodynamics of fluid-crystal interfaces for hard sphere and Yukawa systems to dynamical phenomena such as crystal growth on structured substrates and induced by externally imposed seeds.

1 Introduction

Classical density functional theory (DFT) of inhomogeneous fluids, for reviews see [1–7], has been shown to provide a quantitative unifying theory for freezing in systems with both hard-sphere-like interactions (on the basis of Rosenfeld's fundamental measure theory) [8] and soft-core particles (on the basis of the mean-field approximation) [9]. In principle, DFT represents a microscopic theory which starts from the interparticle interactions and fluid correlations as an input and predicts the crystallisation transition and the full crystal structure (lattice symmetry, lattice constants, Lindemann parameter and its anisotropies). Moreover, DFT can be readily generalized from one-component systems towards binary mixtures.

Attempts to study nucleation and crystal growth within DFT fall into two classes of problems: first, the structure of the critical crystal nucleus both for homogeneous and heterogeneous nucleation can in principle been extracted from conventional (i.e. static) DFT [10]. Second, full-time-dependent problems, such as the growth of a system into a solid microstructure, require a dynamical extension of DFT, the so-called dynamical density functional theory (DDFT). The former problem has mainly been exploited only for nucleation of homogeneous phases (liquid or gas) [11–14] but not

[a] e-mail: schmiedeberg@thphy.uni-duesseldorf.de
[b] e-mail: hlowen@thphy.uni-duesseldorf.de

for *crystal* nucleation. For the latter problem, time-dependent (dynamical) density functional theory was recently developed for Brownian systems such as colloidal suspensions [15–17]. In this mini-review, DDFT is applied to nucleation and growth of crystals.

This mini-review is outlined as follows: we give an introduction to DFT in chapter 2 and present convenient approximations in chapter 3. Dynamical DFT is briefly outlined in chapter 4. Then we apply DFT to crystal-fluid interfaces in equilibrium (chapter 5) and various crystal growth phenomena (chapter 6 and 7). Finally, we conclude in chapter 8.

2 Density functional theory

Density functional theory (DFT) was first invented by Hohenberg and Kohn [18,19] for an inhomogeneous electron gas in 1964. They found a functional for the energy of the system that only depends on the electron density, but which is similar for all external potentials. This approach was generalized to finite temperatures by Mermin [20], and adapted to classical systems by Ebner et al. [21]. Within DFT, the free energy of a system of N classical particles located at positions $\mathbf{r}_i$ with $i = 1, \ldots, N$ is described via the averaged one-particle density given by

$$\rho(\mathbf{r}) = \left\langle \sum_{i=1}^{N} \delta(\mathbf{r} - \mathbf{r}_i) \right\rangle, \tag{1}$$

including the grand canonical ensemble average $\langle\rangle$. At fixed chemical potential μ and temperature T, the grand canonical free energy $\Omega(T, \mu, [\rho(\mathbf{r})])$ can be written as a functional of this one-particle density. Mermin proved that there is a unique grand canonical free energy functional which becomes minimal for the equilibrium one-particle density, i.e.

$$\frac{\delta\Omega[T, \mu, \rho(\mathbf{r})]}{\delta\rho(\mathbf{r})} = 0. \tag{2}$$

Performing a Legendre tansform, the grand canonical free energy functional translates into a Helmholtz free energy functional $\mathcal{F}$ such that it reads

$$\Omega(T, \mu, [\rho(\mathbf{r})]) = \mathcal{F}(T, [\rho(\mathbf{r})]) - \mu \int \mathrm{d}\mathbf{r}\rho(\mathbf{r}). \tag{3}$$

Furthermore, $\mathcal{F}$ can be split up into three parts as

$$\mathcal{F} = \mathcal{F}_{\mathrm{id}} + \mathcal{F}_{\mathrm{ext}} + \mathcal{F}_{\mathrm{exc}}. \tag{4}$$

In this sum, the first term denotes the free energy of an ideal gas which is exactly known [22] as

$$\mathcal{F}_{\mathrm{id}} = k_B T \int \mathrm{d}\mathbf{r}\rho(\mathbf{r}) \left[\ln(\Lambda^3\rho(\mathbf{r})) - 1\right], \tag{5}$$

with the (irrelevant) thermal De Broglie wavelength Λ. The second summand results from the interaction of particles with an external potential $V_{\mathrm{ext}}(\mathbf{r})$ and reads

$$\mathcal{F}_{\mathrm{ext}} = \int \mathrm{d}\mathbf{r}\rho(\mathbf{r})V_{\mathrm{ext}}(\mathbf{r}). \tag{6}$$

Finally, the last term in Eq. (4), called the *excess free energy functional*, is caused by the interactions of particles in the system. In the next section, approximations for

the latter will be pointed out such that the minimization of the grand canonical free energy functional can be computed as

$$\frac{\delta\Omega[\rho(\mathbf{r})]}{\delta\rho(\mathbf{r})} = \frac{\delta\mathcal{F}_{\text{exc}}[\rho(\mathbf{r})]}{\delta\rho(\mathbf{r})} + k_B T\left[\ln(\Lambda^3\rho(\mathbf{r})) + \beta V_{\text{ext}}(\mathbf{r}) - \beta\mu\right] = 0. \tag{7}$$

3 Approximations for the excess functional

The previously described theory requires an expression for an excess free energy functional. One of the exactly known excess free energy functional holds for hard rods in one dimension [23]. In the following, we propose Rosenfeld's fundamental measure approximation [8]. It averages over all possible configurations of the system and by this, e.g., ignores any fluctuations of interfaces and educes only mean-field critical exponents (see [24]).

3.1 Fundamental Measure Theory for hard spheres

Fundamental Measure Theory (FMT) was developed [8] for mixtures of m components of additive hard spheres with diameter σ_i in a three-dimensional system. Here, the interaction potential is defined by

$$\phi_{ij}(r) = \begin{cases} \infty & \text{for } r < \sigma_{ij} \\ 0 & \text{otherwise,} \end{cases} \tag{8}$$

where $\sigma_{ij} = \frac{1}{2}(\sigma_i + \sigma_j)$ for particles of species i (diameter σ_i) and j (diameter σ_j). The derivation of FMT is based on the exact solution of hard rods in one dimension [23] and the exact low density limit. Starting with the latter, the Mayer function $f_{ij}(r) = e^{-\beta\phi_{ij}(r)} - 1$ for hard spheres can be written as

$$f_{ij}(r) = \begin{cases} -1 & \text{for } r < \sigma_{ij} \\ 0 & \text{otherwise,} \end{cases} \tag{9}$$

or as $f_{ij}(r) = -\theta(\sigma_{ij} - r)$ where $\theta(r)$ is the Heaviside step function defined by

$$\theta(x) = \begin{cases} 1 & \text{for } x > 0, \\ 0 & \text{for } x \leq 0. \end{cases} \tag{10}$$

The approach is now to use the *cross-correlation* $\otimes$, which in contrast to the definition of the convolution (cf. Eq. (14)) is given by

$$(f \otimes g)(\mathbf{r} = \mathbf{r}_i - \mathbf{r}_j) = \int \mathrm{d}\mathbf{r}' f(\mathbf{r}' - \mathbf{r}_i) g(\mathbf{r}' - \mathbf{r}_j), \tag{11}$$

to decompose the Mayer function into correlations of weight functions which result from geometrical features as

$$-f_{ij}(r) = \omega_3^i \otimes \omega_0^j + \omega_0^i \otimes \omega_3^j + \omega_2^i \otimes \omega_1^j + \omega_1^i \otimes \omega_2^j - \boldsymbol{\omega}_2^i \otimes \boldsymbol{\omega}_1^j - \boldsymbol{\omega}_1^i \otimes \boldsymbol{\omega}_2^j. \tag{12}$$

The weight functions ω_ν^i are given by

$$\begin{aligned}
\omega_3^i(r) &= \theta(R_i - r),\\
\omega_2^i(r) &= \delta(R_i - r),\\
\omega_1^i(r) &= \frac{1}{4\pi R_i}\omega_2^i(r) = \frac{1}{4\pi R_i}\delta(R_i - r),\\
\omega_0^i(r) &= \frac{1}{4\pi R_i^2}\omega_2^i(r) = \frac{1}{4\pi R_i^2}\delta(R_i - r),\\
\boldsymbol{\omega}_2^i(r) &= \frac{\mathbf{r}}{r}\delta(R_i - r),\\
\boldsymbol{\omega}_1^i(r) &= \frac{1}{4\pi R_i}\boldsymbol{\omega}_2^i(r) = \frac{1}{4\pi R_i}\frac{\mathbf{r}}{r}\delta(R_i - r),
\end{aligned} \tag{13}$$

with R_i denoting the radius of particles of species i ($R_i = \sigma_i/2$). $\delta(x)$ is the well known Dirac delta function and $\theta(x)$ indicates the Heaviside step function. $\omega_\nu^i(r)$ with $\nu = 0, 1, 2, 3$ indicates the four scalar weight functions and $\boldsymbol{\omega}_{(1,2)}^i(r)$ the two vector weight functions. Knowing the weight functions, six weighted densities $n_\nu(\mathbf{r})$ are defined using a convolution $*$ which is

$$(f * g)(\mathbf{r}) = \int \mathrm{d}\mathbf{r} f(\mathbf{r}')g(\mathbf{r} - \mathbf{r}'), \tag{14}$$

such that they read

$$n_\nu(\mathbf{r}) = \sum_{i=1}^{m} \int \mathrm{d}\mathbf{r}' \rho_i(\mathbf{r}')\omega_\nu^i(\mathbf{r} - \mathbf{r}') = \sum_{i=1}^{m} (\rho_i * \omega_\nu^i)(\mathbf{r}), \tag{15}$$

where $\rho_i(\mathbf{r})$ denotes the density distribution of species i. Assuming a homogeneous fluid of only one component with uniform density distribution $\rho(\mathbf{r}) \equiv \rho_b$ and radius R the convolution can be performed analytically such that the resulting weighted densities are $n_3 = \frac{4}{3}\pi R^3\rho_b$, $n_2 = 4\pi R^2\rho_b$, $n_1 = R\rho_b$, and $n_0 = \rho_b$. Each of these weighted (bulk) densities is equal to the bulk density ρ_b times one of the geometrical properties of a sphere: the volume $V = \frac{4}{3}\pi R^3$, the surface area $A = 4\pi R^2$, the radius R and the Euler characteristic. Due to the symmetry of the uniform density distribution, the vectorial weighted densities $\mathbf{n}_2, \mathbf{n}_1$, resulting from anti-symmetric weight functions, vanish. It should be mentioned that, in the general case the latter usually have finite values. These geometrical measures are called the *fundamental measures* leading to the name of the theory.

The excess free energy functional can be assumed to be a combination of the weighted densities, such that the result is of the form

$$\beta\mathcal{F}_{\mathrm{exc}}[\{\rho_i\}] = \int \mathrm{d}\mathbf{r}\Phi(\{n_\nu(\mathbf{r})\}), \tag{16}$$

where $\Phi(\{n_\nu(\mathbf{r})\})$ is given by

$$\Phi(\{n_\nu(\mathbf{r})\}) = f_1(n_3)n_0 + f_2(n_3)n_1n_2 + f_3(n_3)\mathbf{n}_1\cdot\mathbf{n}_2 + f_4(n_3)n_2^3 + f_5(n_3)n_2\mathbf{n}_2\cdot\mathbf{n}_2. \tag{17}$$

Here, Φ is not the interaction potential $\phi(r)$ of Eq. (8) but the *excess free energy density*. Each product of the weighted densities has the dimension $[\mathrm{length}]^{-3}$ corresponding to a density such that the functions $f_j(n_3)$ with $j = 1, \ldots, 5$ need to be

dimensionless and thus, depend only on the dimensionless scalar $n_3(\mathbf{r})$. The functional dependence results from the fact that they have to recover the previously mentioned low density limit truncated after the first term. In order to deduce the $f_j(n_3)$, Rosenfeld started with

$$\lim_{R_i \to \infty} \left(\frac{\mu^i_{\text{exc}}}{V_i} \right) = p, \tag{18}$$

where $V_i = \frac{4}{3}\pi R_i^3$ is the volume of a sphere with radius R_i and p is the pressure in the system. The excess chemical potential μ^i_{exc} can be extracted from the Euler-Lagrange equation Eq. (7) in combination with the ansatz of Eq. (16) to be

$$\mu^i_{\text{exc}} = \frac{\partial \Phi}{\partial \rho_i} = \sum_\nu \frac{\partial \Phi}{\partial n_\nu} \frac{\partial n_\nu}{\partial \rho_i}, \tag{19}$$

with ν denoting the scalar and vectorial functions. In the limit of infinite radii R_i, the only non-vanishing term in Eq. (18) is the first of the sum, such that $p = \frac{\partial \Phi}{\partial n_3}$. Substituting the pressure $p = -\frac{\partial F}{\partial V}$ with $F = \mathcal{F}[\rho]$ from Eqs. (4), (16), and (17) results in a differential equation

$$\frac{\partial \Phi}{\partial n_3} = -\Phi + \sum_\nu \frac{\partial \Phi}{\partial n_\nu} n_\nu + n_0. \tag{20}$$

Solving this yields the prefactors of the excess free energy density $\Phi(\{n_\nu(\mathbf{r})\})$ (17)

$$\begin{aligned} f_1(n_3) &= -\ln(1-n_3), \\ f_2(n_3) &= \frac{1}{1-n_3}, \\ f_3(n_3) &= -\frac{1}{1-n_3}, \\ f_4(n_3) &= \frac{1}{24\pi(1-n_3)^2}, \\ f_5(n_3) &= -\frac{3}{24\pi(1-n_3)^2}. \end{aligned} \tag{21}$$

Integration constants were chosen such that the correct low density behavior is obtained (cf. [7] for details). In conclusion, the excess free energy density can be written as a sum of three parts $\Phi = \Phi_1 + \Phi_2 + \Phi_3$ with

$$\Phi_1 = -n_0 \ln(1-n_3), \tag{22}$$

$$\Phi_2 = \frac{n_1 n_2 - \mathbf{n}_1 \cdot \mathbf{n}_2}{1-n_3}, \tag{23}$$

and

$$\Phi_3 = \frac{n_2^3 - 3 n_2 \mathbf{n}_2 \cdot \mathbf{n}_2}{24\pi(1-n_3)^2}. \tag{24}$$

One year after Rosenfeld, Kierlik and Rosinberg derived a different version of DFT [25] which was shown later [26] to be an alternative deconvolution of the Mayer function with the same results. As both theories fail to treat the freezing transition of single component hard sphere systems, further improvements were necessary. The approach was to reduce the results to lower dimensions in space, due to the fact that a crystal can be interpreted as particles confined to cavities created by

the surrounding particles. This so called *dimensional crossover* [27,28] leads to an empirical modification of the third term in Rosenfeld's excess free energy Φ_3. A further development was then performed by Tarazona and Rosenfeld [29,30] yielding an additional tensorial weight function

$$\hat{\boldsymbol{\omega}}_2^i(r) = \left(\frac{\mathbf{rr}}{r^2} - \frac{\hat{\mathbf{1}}}{3}\right)\omega_2^i(r), \tag{25}$$

including the dyadic product $\mathbf{rr}$ and the unit matrix $\hat{\mathbf{1}}$. Hence, the third term Φ_3 can be amended to

$$\Phi_3 = \left[n_2^3 - 3n_2\mathbf{n}_2\cdot\mathbf{n}_2 + \frac{9}{2}\left(\mathbf{n}_2\hat{\mathbf{n}}_2\mathbf{n}_2 - \mathrm{Tr}(\hat{\mathbf{n}}_2^3)\right)\right]\cdot\frac{1}{24\pi(1-n_3)^2}, \tag{26}$$

where $\mathrm{Tr}(\hat{\mathbf{m}}) = \sum_j m_{jj}$ denotes the classical trace of a matrix $\hat{\mathbf{m}}$ with components m_{ij}.

Indeed, this version of FMT gives a good description of freezing but further improvements have been performed [31,33,34] leading to the White Bear and further White Bear mark II functional which recovers surface tensions [35] or adsorption at walls [34] correctly and will be described in more detail in the following section.

3.2 White Bear and White Bear mark II

In 2002, R. Roth et al. [31] and Y.-X. Yu et al. [32] presented the so-called White Bear version of a fundamental measure density functional. The functional keeps the structure of Rosenfeld's FMT whilst inputting the Mansoori-Carnahan-Starling-Leland bulk equation of state [31]. The structure of the functional follows from the new functions $f_i^{\mathrm{WB}}(n_3) = f_i(n_3)$ for $i \in \{1,2,3\}$ (see Eq. (21)) and $f_5^{\mathrm{WB}}(n_3) = -3f_4^{\mathrm{WB}}(n_3)$ with

$$f_4^{\mathrm{WB}}(n_3) = \frac{n_3 + (1-n_3)^2\log(1-n_3)}{36\pi n_3^2(1-n_3)^2}. \tag{27}$$

Since the result is similar to that one of the White Bear mark II version that will be introduced in the following, both functionals are presented together, only differing in the functions g_2 and g_3 used in Eqs. (29)–(31). For the White Bear version, their values are $g_2^{\mathrm{WB}} = 0$ and

$$g_3^{\mathrm{WB}}(n_3) = \frac{9n_3^2 - 6n_3 - 6(1-n_3)^2\log(1-n_3)}{4n_3^3}. \tag{28}$$

The White Bear version mark II has been introduced by H. Hansen-Goos and R. Roth in the spirit of the White Bear version. It is based on the Carnahan-Starling equation of state and improves upon consistency with an exact scaled-particle theory relation in the case of the pure fluid [33]. The excess free energy density for both White Bear approaches follows with

$$\Phi_1 = -n_0\log(1-n_3), \tag{29}$$

$$\Phi_2 = \left(1 + \frac{1}{9}n_3^2 g_2(n_3)\right)\frac{n_1n_2 - \mathbf{n}_1\cdot\mathbf{n}_2}{1-n_3}, \tag{30}$$

$$\Phi_3 = \left(1 - \frac{4}{9}n_3 g_3(n_3)\right)\frac{n_2^3 - 3n_2\mathbf{n}_2\cdot\mathbf{n}_2}{24\pi(1-n_3)^2}, \tag{31}$$

where for White Bear II the functions g_2 and g_3 are defined by

$$g_2^{\mathrm{WBII}}(n_3) = \frac{6n_3 - 3n_3^2 + 6(1-n_3)\log(1-n_3)}{n_3^3}, \tag{32}$$

$$g_3^{\mathrm{WBII}}(n_3) = \frac{6n_3 - 9n_3^2 + 6n_3^3 + 6(1-n_3)^2\log(1-n_3)}{4n_3^3}. \tag{33}$$

Of course, the tensorial weight function (see Eq. (25)), introduced by P. Tarazona, can be applied. And due to the construction of the functional, its fluid properties follow directly from the Carnahan-Starling results, like its excess free energy.

3.3 Fundamental Measure Theory for hard disks

At first glance, it is a confusing feature of the original approach of Rosenfeld, that it well describes three-dimensional systems but fails for two dimensions [36,37]. For the latter the exact deconvolution of the Mayer function (see Eq. (12)) requires an infinite number of weight functions [38,39]. In this section a recent approach [40] will be sketched out to obtain a density functional which describes the hard disk solid phase in an appropriate way. The path to follow was explained by Tarazona and Rosenfeld [29,41] already more than twenty years ago. The Gauss-Bonnet theorem is used to perform the deconvolution of the Mayer function in analogy to Eq. (12) but with an additional tensorial term, similar to the one in the improved three-dimensional functional. This results in

$$-f_{ij}(r) \approx \omega_2^i \otimes \omega_0^j + \omega_0^i \otimes \omega_2^j + C_0\omega_1^i \otimes \omega_1^j + C_1\boldsymbol{\omega}_1^i \otimes \boldsymbol{\omega}_1^j + C_2\hat{\boldsymbol{\omega}}_1^i \otimes \hat{\boldsymbol{\omega}}_1^j + ..., \tag{34}$$

with $C_0 = \pi/2$, $C_1 = -1$, and $C_2 = -\pi/4$, and the weight functions given in analogy to Eq. (13) by

$$\begin{aligned}
\omega_2^i(r) &= \theta(R_i - r),\\
\omega_1^i(r) &= \delta(R_i - r),\\
\omega_0^i(r) &= \frac{1}{\pi\sigma_i}\omega_1^i(r) = \frac{1}{\pi\sigma_i}\delta(R_i - r),\\
\boldsymbol{\omega}_1^i(r) &= \frac{\mathbf{r}}{r}\omega_1^i(r) = \frac{\mathbf{r}}{r}\delta(R_i - r), \text{and}\\
\hat{\boldsymbol{\omega}}_1^i(r) &= \frac{\mathbf{rr}}{r^2}\omega_1^i(r) = \frac{\mathbf{rr}}{r^2}\delta(R_i - r).
\end{aligned} \tag{35}$$

Similar to the three-dimensional case, the first three weight functions are scalars, whereas $\boldsymbol{\omega}_1^i(r)$ is a vector and $\hat{\boldsymbol{\omega}}_1^i(r)$ is a matrix containing the dyadic product $\mathbf{rr}$.

As in the three-dimensional system, the excess free energy $\mathcal{F}_{\mathrm{exc}}$ can be expressed by the integral of the excess free energy density Φ (see Eq. (16)). Φ is assumed to be a linear combination of weight functions $n_\nu = \sum_i(\rho_i * \omega_\nu^i)$,

$$\Phi = f(n_2)n_0 + g_0(n_2)\tilde{C}_0(n_1)^2 + g_1(n_2)\tilde{C}_1\mathbf{n}_1 \cdot \mathbf{n}_1 + g_2(n_2)\tilde{C}_2\mathrm{Tr}(\hat{\mathbf{n}}_1^2), \tag{36}$$

where f and g_j, $(j = 0, 1, 2)$ depend only on the packing fraction n_2. Hence, the ansatz is the same as Rosenfeld's in Eq. (18), so that with $g_j \equiv g$, Φ becomes

$$\Phi = -n_0\ln(1-n_2) + \frac{1}{4\pi(1-n_2)}\left[\tilde{C}_0(n_1)^2 + \tilde{C}_1\mathbf{n}_1 \cdot \mathbf{n}_1 + \tilde{C}_2\mathrm{Tr}(\hat{\mathbf{n}}_1^2)\right]. \tag{37}$$

The remaining work is now to find the coefficients $\tilde{C}_l$ $(l = 0, 1, 2)$ such that Φ on the one hand recovers the correct second virial coefficient and on the other hand describes the low density limit correctly. Resulting from this two equations $2C_0 + C_1 = 2$ and $C_0 + C_1 + C_2 = 0$ can be written down and solved with a parameter b as

$$\tilde{C}_0 = \frac{b+2}{3}, \qquad \tilde{C}_1 = \frac{b-4}{3}, \text{ and } \tilde{C}_2 = \frac{2-2b}{3}, \tag{38}$$

where b is chosen such that the results fit best to the Mayer function. The optimized value of $b = \frac{11}{4}$ leads to the concluding excess free energy density given by

$$\Phi = -n_0 \ln(1-n_2) + \frac{1}{4\pi(1-n_2)} \left(\frac{19}{12}(n_1)^2 - \frac{5}{12}\mathbf{n}_1 \cdot \mathbf{n}_1 - \frac{7}{6}\mathrm{Tr}(\hat{\mathbf{n}}_1^2) \right). \tag{39}$$

4 Dynamical density functional theory

The dynamical behavior of many body systems is interesting to study especially its possible connection to equilibrium properties. Several approaches have been made to describe the density dependence on time $\rho(\mathbf{r}, t)$ since the 1970s [22,42,43]. Based on the theory of spinodal decomposition [44], a particle current $\mathbf{j}(\mathbf{r}, t)$ due to a spatial gradient of the chemical potential μ is assumed as

$$\mathbf{j}(\mathbf{r}, t) = -\Gamma \rho(\mathbf{r}, t) \nabla \mu(\mathbf{r}, t), \tag{40}$$

with a time-dependent density distribution $\rho(\mathbf{r}, t)$, a chemical potential $\mu(\mathbf{r}, t)$, and a mobility constant Γ. Linking the results to equilibrium DFT, the gradient can be expressed by a functional derivative (compare with Eq. (7)) as

$$\mu(\mathbf{r}, t) = \frac{\delta \mathcal{F}_{\mathrm{exc}}[\rho(\mathbf{r}, t)]}{\delta \rho(\mathbf{r}, t)} + V_{\mathrm{ext}}(\mathbf{r}, t). \tag{41}$$

In combination with the continuity equation

$$\frac{\partial \rho(\mathbf{r}, t)}{\partial t} = -\nabla \cdot \mathbf{j}(\mathbf{r}, t), \tag{42}$$

a basis for a dynamical density functional theory (DDFT) is given such that the DDFT equation reads

$$\frac{\partial \rho(\mathbf{r}, t)}{\partial t} = \Gamma \nabla \left[\rho(\mathbf{r}, t) \nabla \frac{\delta \Omega[\rho(\mathbf{r}, t)]}{\delta \rho(\mathbf{r}, t)} \right]. \tag{43}$$

5 Hard sphere crystal-fluid interface

FMT can be applied to determine the orientation-resolved interfacial tension as well as stiffness for the equilibrium hard sphere crystal-fluid interface relying on excellent bulk freezing data [45]. The White Bear mark II functional was used and the results were compared with Monte Carlo simulations [35]. Data for the resulting density profiles are shown in Fig. 1 where the three-dimensional density profile $\rho(x, y, z)$ is laterally integrated resulting in an effective one-dimensional profiles

$$\bar{\rho}(z) = \frac{1}{L_x L_y} \int_0^{L_x} \int_0^{L_y} \rho(x, y, z) \mathrm{d}y \mathrm{d}x, \tag{44}$$

with L_x and L_y denoting the lengths of the simulation box in x- and y-direction.

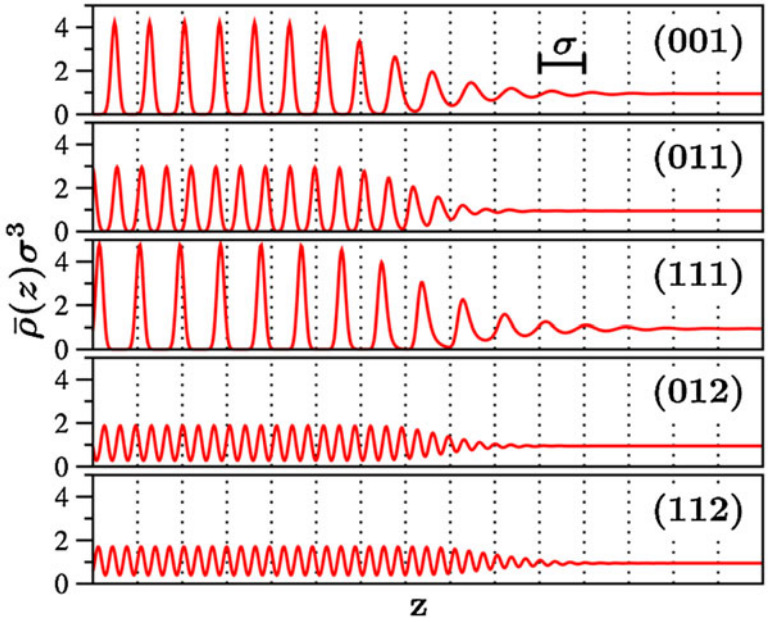

Fig. 1. DFT results: Laterally integrated density profiles $\bar{\rho}(z)$ for the five surface orientations, as indicated. The periodic length of the total profiles in z direction is 50.15σ (001), 53.19σ (011), 65.15σ (111), 56.07σ (012), and 61.42σ (112) (for figure and more details see [35]).

Depending on the orientation of the interface with respect to the fcc-crystal (as indicated by the Miller indices in Fig. 1), the density profiles slightly differ in amplitude and frequency of the peaks. From these density profiles interfacial tension and stiffness were extracted. The microscopic DFT predicts a tension of $0.66k_BT/\sigma^2$ with a small anisotropy of about $0.025k_BT$. Furthermore stiffnesses were computed with, e.g., $0.53k_BT/\sigma^2$ for the (001) orientation, or $1.03k_BT/\sigma^2$ for the (111) orientation. All results were confirmed by simulations and additionally compared with experimental results [35].

6 Heterogeneous crystallization in 2d on patterned substrates

6.1 Static DFT

Recently, a two-dimensional system of hard disks influenced by a substrate potential was explored [46]. By inducing an external potential with square symmetry, an incompatibility is caused compared to the symmetry preferred by the particles which is triangular (with quasi-long range order) [47] at sufficiently high densities. The lattice constant of the substrate potential is chosen such that on average exactly one particle is located at each minimum of the substrate. In the following, the phase behavior is determined depending on the packing fraction η and the strength of the particle-substrate interaction V_0 and shown in Fig. 2. The substrate potential is modeled by

$$V_{\text{ext}}(\mathbf{r}) = V_0\left(1 - \frac{1}{4}\left|\sum_{j=1}^{4} e^{i\mathbf{k}_j\cdot\mathbf{r}}\right|^2\right), \tag{45}$$

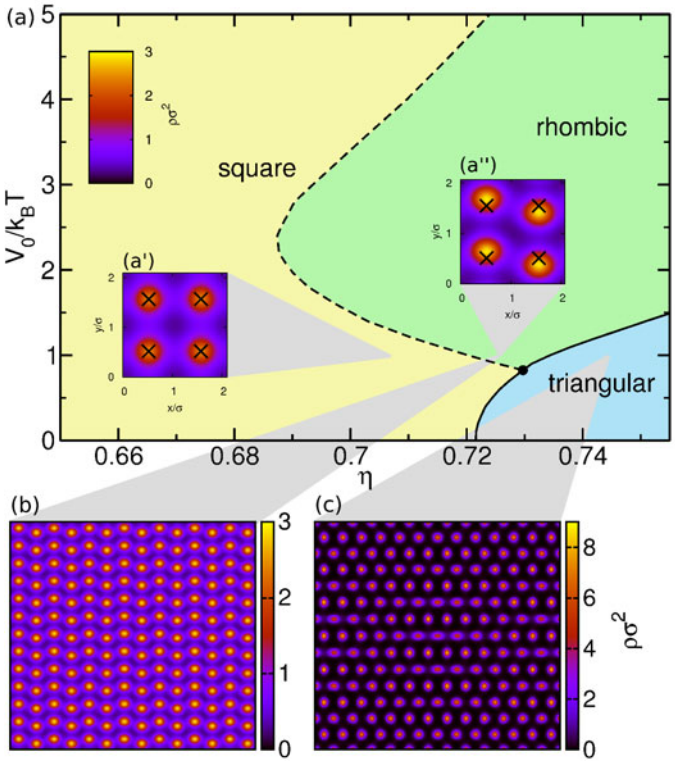

Fig. 2. (a) Phase diagram for hard disks on a square-substrate showing the three different phases, square modulated fluid, rhombic, and triangular crystal. The dashed line indicates the second order and the solid line the first order phase transition, where the dot denotes the triple point. Density contour plots of the three phases are included obtained for a fixed external potential with $V_0/k_BT = 1$ and packing fractions (a′) $\eta = 0.7069$, [(a″), (b)] $\eta = 0.7257$, and (c) $\eta = 0.7383$ (for figure and more details see [46]).

with the four reciprocal lattice vectors $\{\mathbf{k}_j\} = \{(\pm 1, \pm 1)\frac{\pi}{a}\}$, and the lattice constant a of the substrate square lattice. Due to the restriction of unit filling, the areal number density $1/a^2$ corresponds to the dimensionless packing fraction $\eta = \pi\sigma^2/4a^2$ of the system.

In the absence of an external potential ($V_0 = 0$), the bulk freezing transition is recovered which is first order in this theory [7]. At low packing fractions but non-vanishing interaction strength V_0, the particles locate on average at the minima positions of the substrate potential (see (a′)) indicated by black crosses. The first order phase transition to the triangular crystalline phase shifts to higher packing fractions. A density contour plot of the slightly distorted hexagonal crystal is depicted in Fig. 2(c). Upon a reduced amplitude of $V_0/k_BT = 0.82$, a rhombic order can be observed prior the triangular phase. As shown in Figs. 2(a″, b), the columns of particles are dislocated alternatingly – all even numbered columns are dislocated in one while all odd numbered columns are shifted oppositely. The square-to-rhombic transition can in principle be continuous in analogy to a Martensitic transition [48] but our DFT calculations show a second order fluid phase transition. Increasing the interaction strength at intermediate packing fractions, a reentrant effect of the rhombic phase is seen. This results from the interplay of the substrate potential with entropy. If the interaction is weak, the fluid is slightly modulated but hardly perturbed due

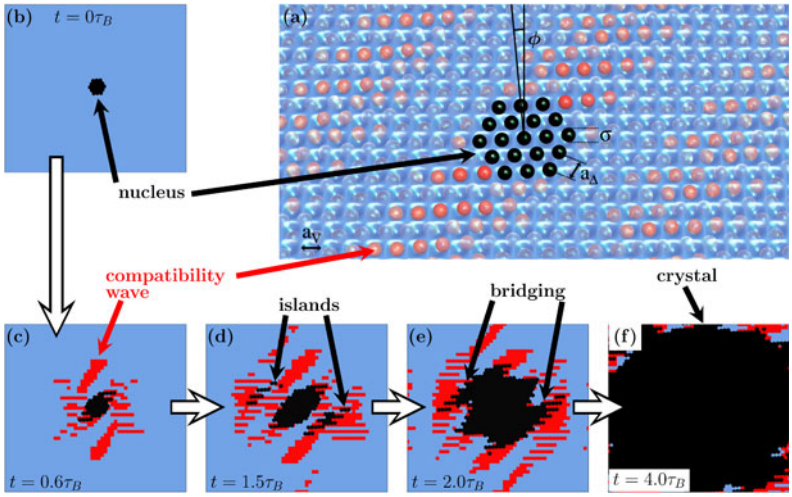

Fig. 3. (a) Schematic representation of a nucleus of hard disks with diameter σ located on a two-dimensional substrate with square symmetry rotated counterclockwise by an angle $\phi = 5^\circ$ relative to a symmetry direction of the substrate and lattice constant a_V. The snapshots (b)-(f) illustrate the growth of a spherical nucleus influenced by the substrate with amplitude $V_0 = 0.5k_BT$ at times (b) $t = 0.0$, (c) $t = 0.6\tau_\mathrm{B}$, (d) $t = 1.5\tau_\mathrm{B}$, (e) $t = 2.0\tau_\mathrm{B}$, and (f) $t = 4.0\tau_\mathrm{B}$, where τ_B is the Brownian time. Red regions display the compatibility wave and are defined by density peaks above a threshold value $\rho_\mathrm{th}\sigma^2 = 1.5061$. Black regions denote crystalline areas ($\rho_\mathrm{th}\sigma^2 = 2.0$), whereas blue regions remain fluid ($\rho_\mathrm{th}\sigma^2 \leq 1.5060$) (for figure and more details see [49]).

to the external potential. For larger interactions, entropy which is mainly limited by nearest neighbor interactions dominates the phase behavior. It can be increased by dislocating the particles to the rhombic order. At very high amplitudes, the substrate pins the particles strongly to the minima position suppressing all fluctuations. Consequently, a square phase is obtained again.

These results can be compared with Monte Carlo simulations which confirm the DFT predictions. Only the order of the square-to-rhombic transition is underestimated by our DFT calculations but nevertheless, simulations still show a transition, which has a clear structural signature, but no thermodynamic footprint [46].

6.2 Dynamics of crystal growth

By using DDFT, the dynamics of two-dimensional crystal growth on a patterned substrate with square symmetry was studied [49]. A few-particle nucleus is placed on a structured template such that crystallization was observed. In analogy to the static case, there is a competition between the hexagonal symmetry hard disks prefer to arrange in and the square symmetry induced by the substrate. Resulting from this, a new crystal growth scenario occurs. In a bulk systems where no external substrate is present, a well-defined as well as connected crystal-fluid interface is seen. In contrast, in the presence of a structured substrate, crystal growth is driven by a "compatibility wave" which dictates the efficiency and the growth direction.

In Fig. 3, a schematic representation of this slightly rotated nucleus on top of the square substrate of Eq. (45) is shown, as well as an examplary growth process. Red colored regions display the compatibility wave on top of which first transient crystalline islands form (black regions). In a next step, there is a bridge formation

such that the islands are perfectly linked with the original crystal during the further growth process. Consequently, no connected crystal-fluid interface is observed in this case but positions where the minima of the substrate potential are compatible with the positions of the grown crystal occur earlier than in less compatible regions.

The validity of this growth scenario via a compatibility wave was shown for a large class of different substrate symmetries [49] including quasicrystalline patterns.

7 Further developments

7.1 From hard spheres to soft interactions

Similar studies were performed for soft interactions. In this case, however, there is no equivalent to the FMT functional such that more crude approximations like the Ramakrishnan-Yussouff (RY) theory are typically employed [50] which needs a high-precision fluid direct correlation function as an input. In two spatial dimensions, crystallization phenomena were intensely studied for dipolar interactions where the repulsive interaction pair potential scales with the inverse cube of the interparticle distance [51]. This was also extended towards binary mixtures [52–54].

In three dimensions, a RY density functional study for the bcc-fluid interface of three-dimensional Yukawa systems was performed to access the interfacial structure and free energy [55]. DFT predicts an interfacial free energy of $0.12k_BT/a^2$ with a denoting the mean interparticle spacing, which is independent of the screening strength. This value is in reasonable agreement with computer simulations. Hence, in the Yukawa system, bcc crystal-fluid free energies are a factor of about 3 smaller than face-centered-cubic crystal-fluid free energies [35]. Applications to other soft potentials like inverse-power-laws are still lying ahead in three dimensions.

7.2 The role of substrate curvature in heterogeneous crystallization

Recently, the role of substrate curvature on heterogeneous nucleation was systematically studied on the fundamental particle level [56] using simultaneously Brownian dynamics computer simulations of hard spheres and confocal microscopy experiments on sterically-stabilized colloidal suspensions [57], extending previous work for planar substrates [60]. The following scenario was detected: first a critical crystalline nucleus is formed at the substrate which then grows further. The crystalline nucleus stores elastic stress induced by the substrate curvature and grows until a limiting size is reached upon which the nucleus detaches from the substrate. After detachment, the elastic stress is released and the undistorted nucleus grows further, refreezing at the substrate. This scenario in its early stage is compatible with previous simulations [61] but contradicts a catalytic mechanism where subsequent crystal nuclei are generated one after the other. The detachment size scales with the substrate curvature as predicted by a simple scaling law derived from macroscopic elasticity theory. Although the data of Ref. [57] were obtained for overcompressed hard sphere suspensions, the scenario is expected to be general. More details are presented in [58] of this special issue.

7.3 Interfaces between coexisting liquid crystalline phases

Recently, the traditional phase-field-crystal model (for a discussion, see [59]) was extended towards liquid crystalline phases with orientational degrees of freedom [62–64],

for a review see [65]. Previous theories [66,67] were extended to include also liquid-crystalline phases which exhibit translational crystalline order. In two spatial dimensions, both the interfaces separating the plastic-crystalline phase and the isotropic and columnar phase were computed by using the extended phase-field crystal model of Ref. [62] and the structural anisotropic was determined. As a general finding, the width of the interface with respect to the nematic order parameter characterizing the orientational order is larger than the width of the mean-density interface. In approaching the interface from the PTC side, at first, the mean density goes down, and then the nematic order parameter follows (compare to [68] for the fluid-crystal interface). The relative shift in the two profiles is larger than a full lattice constant of the plastic crystal. These predictions for the interfacial profiles can, in principle, be verified in real-space experiments of rod-like colloidal dispersions. Another study of Fundamental Measure DDFT for anisotropic particles was performed in [69].

7.4 Vacancy diffusion in colloidal crystals

A two-dimensional crystal of repulsive dipolar particles was studied in the vicinity of its melting transition by using Brownian dynamics computer simulation, dynamical density-functional theory, and phase-field-crystal modeling [70]. A vacancy is created by taking out a particle from an equilibrated crystal, and the relaxation dynamics of the vacancy is followed by monitoring the time-dependent one-particle density. The vacancy was quickly filled up by diffusive hopping of neighboring particles towards the vacancy center. The diffusion constant decreases with decreasing temperature in the simulations. This trend is reproduced by the dynamical density functional theory. Conversely, the phase-field-crystal calculations predict the opposite trend. Therefore, importantly, the phase-field model needs a temperature-dependent expression for the mobility to predict trends correctly.

7.5 Generalizations and applications of dynamical density functional theory

The dynamical density functional theory was extended to other situations including mixtures and temperature gradients [71] by using the projection operator technique [72] and incorporating the local temperature field as another slow dynamical variable. Also the entropy density was considered to be a relevant variable in order to establish a microscopic approach to entropy production [73]. Still applications to include the microscopic momentum density are needed in order to generalize dynamical density functional theory to molecular systems (like metals) rather than colloidal suspensions in an overdamped solvent.

8 Conclusions

This mini-review summarizes recent progress in the description of density functional theory (DFT) of heterogenous crystallization. An almost complete picture arises for two spatial dimensions, where DFT can be numerically solved completely both for various static and dynamic problems for hard disks and soft interactions. In particular, the role of crystalline seeds can be explored (see also [74]) and the crystallization process on a patterned substrate was unravelled.

In three spatial dimensions the numerical effort is much higher, buth solid-fluid interfaces were calculated both for hard spheres and Yukawa interactions with reasonable interfacial tensions. The big challenge is to do time-dependent DDFT in three

dimensions. With further increasing computational power, many more interesting aspects of crystallization will be explored in the future including crystal growth [75] and glass formation [76,77] in various external fields and for liquid crystalline systems.

We thank M. Oettel, R. Rozas, S. Egelhaaf, J. Horbach, A. Voigt, and H. Emmerich for the fruitful collaboration within the SPP 1296. This work was supported by the DFG via SPP 1296.

References

1. Y. Singh, Phys. Rep. **207**, 351 (1991)
2. H. Löwen, Phys. Rep. **237**, 249 (1994)
3. J. Wu, AIChE J. **52**, 1169 (2006)
4. P. Tarazona, J.A. Cuesta, Y. Martinez-Raton, *Density Functional Theories of Hard Particle Systems* (Springer Berlin/Heidelberg, 2008)
5. G. Kahl, H. Löwen, J. Phys. **21**, 464101 (2009)
6. J.F. Lutsko, Adv. Chem. Phys. **144**, 1 (2010)
7. R. Roth, J. Phys. **22**, 063102 (2010)
8. Y. Rosenfeld, Phys. Rev. Lett. **63**, 980 (1989)
9. A.J. Archer, Phys. Rev. E **72**, 051501 (2005)
10. D.W. Oxtoby, *Liquids, Freezing and the Glass Transition* (North Holland, Amsterdam, 1991)
11. V. Talanquer, D.W. Oxtoby, J. Chem. Phys. **104**, 1993 (1996)
12. I. Napari, A. Laaksonen, J. Chem. Phys. **111**, 5485 (1999)
13. B. Husowitz, V. Talanquer, J. Chem. Phys. **122**, 194710 (2005)
14. T.V. Bykov, X.C. Zeng, J. Chem. Phys. **125**, 144515 (2006)
15. U.M.B. Marconi, P. Tarazona, J. Chem. Phys. **110**, 8032 (1999)
16. U.M.B. Marconi, P. Tarazona, J. Phys. **12**, A413 (2000)
17. A.J. Archer, R. Evans, J. Chem. Phys. **121**, 4246 (2004)
18. P. Hohenberg, W. Kohn, Phys. Rev. **136**, B864 (1964)
19. W. Kohn, *Nobel Lecture: Electronic Structure of Matter – Wave Functions and Density Functionals* (World Scientific Publishing Co., Singapore, 2003)
20. N.D. Mermin, Phys. Rev. **137**, A1441 (1965)
21. C. Ebner, W.F. Saam, D. Stroud, Phys. Rev. A **14**, 2264 (1976)
22. R. Evans, Adv. Phys. **28**, 143 (1979)
23. J.K. Percus, J. Stat. Phys. **15**, 505 (1976)
24. R.L.C. Vink, T. Neuhaus, H. Löwen, J. Chem. Phys. **134**, 204907 (2011)
25. E. Kierlik, M.L. Rosinberg, Phys. Rev. A **42**, 3382 (1990)
26. S. Phan, E. Kierlik, M.L. Rosinberg, B. Bildstein, G. Kahl, Phys. Rev. E **48**, 618 (1993)
27. Y. Rosenfeld, M. Schmidt, H. Löwen, P. Tarazona, J. Phys. **8**, L577 (1996)
28. Y. Rosenfeld, M. Schmidt, H. Löwen, P. Tarazona, Phys. Rev. E **55**, 4245 (1997)
29. P. Tarazona, Y. Rosenfeld, Phys. Rev. E **55**, R4873 (1997)
30. P. Tarazona, Phys. Rev. Lett. **84**, 694 (2000)
31. R. Roth, R. Evans, A. Lang, G. Kahl, J. Phys. **14**, 12063 (2002)
32. Y.-X. Yu, J. Wu, J. Chem. Phys. **117**, 10156 (2002)
33. H. Hansen-Goos, R. Roth, J. Phys. **18**, 8413 (2006)
34. H. Hansen-Goos, R. Roth, J. Chem. Phys. **124**, 154506 (2006)
35. A. Härtel, M. Oettel, R.E. Rozas, S.U. Egelhaaf, J. Horbach, H. Löwen, Phys. Rev. Lett. **108**, 226101 (2012)
36. E. Kierlik, M.L. Rosinberg, Phys. Rev. A **44**, 5025 (1991)
37. Y. Rosenfeld, J. Chem. Phys. **98**, 8126 (1993)
38. H. Hansen-Goos, K. Mecke, Phys. Rev. Lett. **102**, 018302 (2009)
39. H. Hansen-Goos, K. Mecke, J. Phys. **22**, 364107 (2010)
40. R. Roth, K. Mecke, M. Oettel, J. Chem. Phys. **136**, 081101 (2012)

41. P. Tarazona, Y. Rosenfeld, Free Energy Density Functional From 0D Cavities in *New Approaches to Problems in Liquid State Theory Inhomogeneities and Phase Separation in Simple, Complex and Quantum Fluids*, edited by C. Caccamo, J.-P. Hansen, G. Stell, NATO Sci. Ser. C 529 (Springer Netherlands, 1998), p. 293
42. D. Henderson, F.F. Abraham, J.A. Barker, Mol. Phys. **31**, 1291 (1976)
43. M.M. Telo Da Gama, R. Evans, Mol. Phys. **38**, 367 (1979)
44. J.W. Cahn, J. Chem. Phys. **42**, 93 (1965)
45. M. Oettel, S. Görig, A. Härtel, H. Löwen, M. Radu, T. Schilling, Phys. Rev. E **82**, 051404 (2010)
46. T. Neuhaus, M. Marechal, M. Schmiedeberg, H. Löwen, Phys. Rev. Lett. **110**, 118301 (2013)
47. A.C. Mitus, H. Weber, D. Marx, Phys. Rev. E **55**, 6855 (1997)
48. J.A. Weiss, D.A. Oxtoby, D.G. Grier, C.A. Murray, J. Chem. Phys. **103**, 1180 (1995)
49. T. Neuhaus, M. Schmiedeberg, H. Löwen, New J. Phys. **15**, 073013 (2013)
50. T.V. Ramakrishnan, M. Yussouff, Phys. Rev. B **19**, 2775 (1979)
51. S. van Teeffelen, C.N. Likos, H. Löwen, Phys. Rev. Lett. **100**, 108302 (2008)
52. L. Assoud, F. Ebert, P. Keim, R. Messina, G. Maret, H. Löwen, Phys. Rev. Lett. **102**, 238301 (2009)
53. L. Assoud, F. Ebert, P. Keim, R. Messina, G. Maret, H. Löwen, J. Phys. **21**, 464114 (2009)
54. L. Assoud, R. Messina, H. Löwen, Mol. Phys. **109**, 1385 (2011)
55. V. Heinonen, A. Mijailovic, C.V. Achim, T. Ala-Nissila, R.E. Rozas, J. Horbach, H. Löwen, J. Chem. Phys. **138**, 044705 (2013)
56. A. Ivlev, G. Morfill, H. Löwen, *Complex Plasmas and Colloidal Dispersions: Particle-Resolved Studies of Classical Liquids and Solids* (World Scientific, 2012)
57. E. Allahyarov, K. Sandomirski, S.U. Egelhaaf, H. Löwen (submitted) (2013)
58. K. Sandomirski, S. Walta, J. Dubbert, E. Allahyarov, A.B. Schofield, H. Löwen, W. Richtering, S.U. Egelhaaf, Eur. Phys. J. Special Topics **223**(3), 439 (2014)
59. R. Backofen, A. Voigt, Eur. Phys. J. Special Topics **223**(3), 497 (2014)
60. T. Vissers, A. Wysocki, M. Rex, H. Löwen, C.P. Royall, A. Imhof, A. van Blaaderen, Soft Matter **7**, 2352 (2011)
61. A. Cacciuto, S. Auer, D. Frenkel, Nature **428**, 404 (2004)
62. H. Löwen, J. Phys. **22**, 364105 (2010)
63. R. Wittkowski, H. Löwen, H.R. Brand, Phys. Rev. E **82**, 031708 (2010)
64. E. Granato, J.A.P. Ramos, C.V. Achim, J. Lehikoinen, S.C. Ying, T. Ala-Nissila, K.R. Elder, Phys. Rev. E **84**, 031102 (2011)
65. H. Emmerich, H. Löwen, R. Wittkowski, T. Gruhn, G.I. Tóth, G. Tegze, L. Gránásy, Adv. Phys. **61**, 665 (2012)
66. S. van Teeffelen, R. Backofen, A. Voigt, H. Löwen, Phys. Rev. E **79**, 051404 (2009)
67. M.A. Choudhary, D. Li, H. Emmerich, H. Löwen, J. Phys. **23**, 265005 (2011)
68. H. Löwen, T. Beier, H. Wagner, Europhys. Lett. **9**, 791 (1989)
69. A. Härtel, R. Blaak, H. Löwen, Phys. Rev. E **81**, 051703 (2010)
70. S. van Teeffelen, C.V. Achim, H. Löwen, Phys. Rev. E **87**, 022306 (2013)
71. R. Wittkowski, H. Löwen, H.R. Brand, J. Chem. Phys. **137**, 224904 (2012)
72. P. Español, H. Löwen, J. Chem. Phys. **131**, 244101 (2009)
73. R. Wittkowski, H. Löwen, H.R. Brand, J. Phys. A **46**, 355003 (2013)
74. T. Neuhaus, M. Schmiedeberg, H. Löwen, Phys. Rev. E **88**, 062316 (2013)
75. E. Villanova-Vidal, T. Palberg, H.J. Schöpe, H. Löwen, Philos. Mag. **89**, 1695 (2009)
76. C. Renner, H. Löwen, J.L. Barrat, Phys. Rev. E **52**, 5091 (1995)
77. T. Fehr, H. Löwen, Phys. Rev. E **52**, 4016 (1995)